(Received 2 May 2025, Accepted 17 June 2025, Scheduled 30 June 2025)

Low-Loss Microstrip Tri-Band Differential Bandpass Filters Using a Non-Edge-Coupled Structure

Chuan Shao[1, 2, *], Yang Li[3], Liang Wang[3], Rong Cai[1, 2], and Kai Xu[4]

[1]*School of Information Engineering, Jiangsu College of Engineering and Technology, Nantong 226000, Jiangsu, China*
[2]*Nantong Key Laboratory of Artificial Intelligence New Quality Technology Jiangsu College of Engineering and Technology, Nantong 226000, Jiangsu, China*
[3]*Jiangsu Vocational College of Business, China*
[4]*Research Center for Intelligent Information Technology, Nantong University, Nantong 226019, China*

ABSTRACT: In this paper, a novel differential tri-band bandpass filter with a low-loss characteristic and high selectivity is proposed. The low-loss feature is attributed to the non-coupled structure, which circumvents the additional radiation losses from coupling slots. Furthermore, the excellent isolation and significantly enhanced selectivity between passbands are achieved via the inherent transmission zeros among them. Three desirable differential operating passbands can be conveniently allocated by adjusting the impedance ratios of the tri-section stepped impedance resonators. Consequently, the proposed filter design demonstrates a straightforward and efficient design methodology. To validate the feasibility of this approach, a differential tri-band bandpass with passbands at 1.35 GHz, 4.5 GHz, and 7.6 GHz was constructed and experimentally verified. The measured minimum insertion losses were 0.15 dB, 0.5 dB, and 1.2 dB, respectively, indicating high performance. Specifically, the roll-off rates of the lower and upper edges of the three passbands are as follows: for the first passband, 30 dB/GHz and 23 dB/GHz; for the second passband, 27 dB/GHz and 25 dB/GHz; and for the third passband, 24 dB/GHz and 29 dB/GHz. The achieved concordance between simulated and measured results confirms the practicality and viability of this design for advanced communication systems.

1. INTRODUCTION

In recent years, differential bandpass filters have garnered significant attention due to their superior immunity to environmental noise and interference compared to single-ended counterparts [1–4]. Besides, as multi-band operation becomes increasingly common in modern wireless communication systems, the demand for compact, high-performance differential multi-band bandpass filters has surged. These filters are essential for enhancing differential-mode performance and anti-noise capabilities, making them crucial components in high-efficiency RF/microwave transceivers. For dual-band applications, differential dual-band bandpass filters based on coupled stepped-impedance resonators (SIRs) and stub-loaded resonators (SLRs) have been both introduced and extensively investigated [5, 6]. In the realm of tri-band applications, differential tri-band bandpass filters have been initially conceptualized and developed utilizing SLRs or square ring loaded resonators [7–9]. Given the proximity of the differential and common-mode resonant frequencies, the common-mode suppression of the afore-mentioned differential bandpass filter typically ranges around 20 dB. In order to enhance the common-mode suppression of tri-band differential bandpass filters, researchers have proposed hybrid structures that integrate microstrip lines with slot lines [10–12]. As is well known, slot lines are inherently unable to support common-mode propagation, thus endowing the differential filters with this configuration to exhibit superior common-mode rejection characteristics. However, the incorporation of slot-line structures results in the filters lacking a complete ground plane, which poses significant challenges in encapsulating these filters within a metallic enclosure. Consequently, this limitation greatly restricts the applicability of such filters in practical applications.

Generally, the design of microwave passive components, such as filters [13, 14], power dividers [15, 16], and couplers [17, 18], typically does not focus on their loss characteristics. The main sources of insertion loss in these passive components are conductor losses, dielectric losses, and radiation losses. However, in practical microwave communication systems, passive elements with lower loss are significantly more preferred. The high-temperature super-conducting (HTS) technology has emerged as a promising solution to overcome these losses and develop RF/microwave bandpass filters with excellent performance, such as extremely low loss and very sharp skirt rejections. This advantage is attributable to the extremely low surface resistance of HTS materials, which enables HTS filters to achieve low-loss characteristics [19, 20]. However, the application of HTS technology also faces several challenges, including complex cooling requirements, high fabrication costs, and potential issues with mechanical stability and reliability. Despite significant progress in filter design as reported in [1–20], several key issues remain unaddressed. For instance, while most studies have focused on reducing circuit size, increasing device bandwidth, and using special

* Corresponding author: Chuan Shao (ch_shao@126.com).

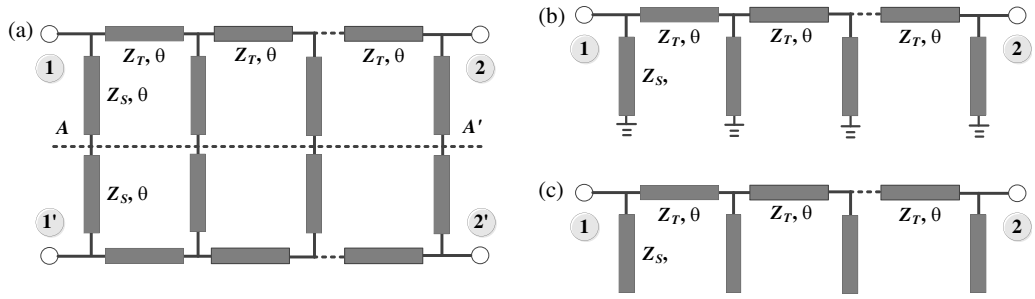

FIGURE 1. Transmission-line schematic of traditional branch-line differential bandpass filter. (a) Overall differential bandpass filter. (b) and (c) Differential and common-mode half bisections of the differential bandpass filter.

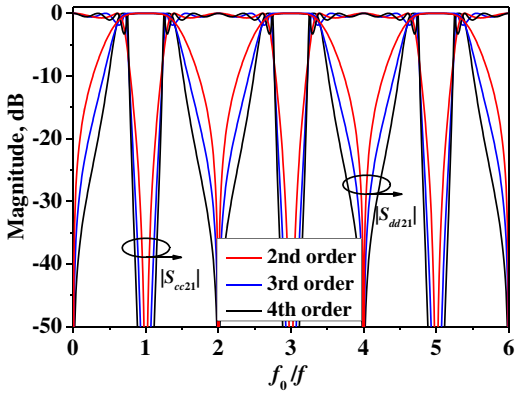

FIGURE 2. Transmission coefficients of bisections shown in Figure 1(b) and (c) with different filter order ($Z_T = 50\,\Omega$, $Z_S = 50\,\Omega$).

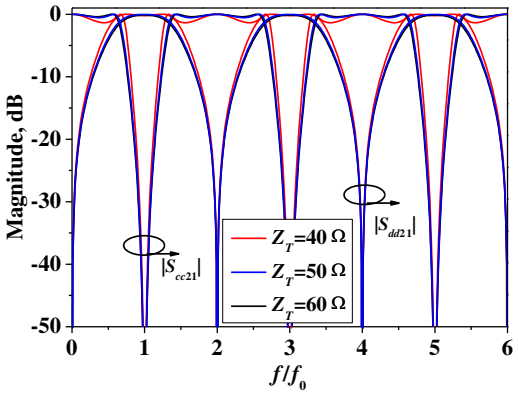

FIGURE 3. Transmission coefficients of bisections shown in Figure 1(b) and (c) with different values of Z_T ($Z_S = 50\,\Omega$).

processes to achieve lower insertion loss, there has been little research on designing microwave passive devices based on the analysis of transmission line radiation characteristics under ordinary printed circuit board (PCB) process in terms of ease of fabrication and cost-effectiveness.

In this paper, a low-loss differential tri-band bandpass filter constructed by a pair of tri-section stepped impedance resonators is presented. The proposed differential filter shows a simple and effective design process. Four inherently generated transmission zeros in the operation band have greatly improved the selectivity and the isolation among these three passbands. The proposed differential filter is designed using a non-edge-coupled structure, thus avoiding additional radiation losses. Additionally, the absence of narrow coupling gaps eliminates unnecessary fabrication tolerances, resulting in an excellent match between the simulation and measurement results. The proposed filter's characteristics make it suitable for applications in advanced communication systems where high selectivity and low loss are required, such as in 5G/6G networks, satellite communications, and radar systems.

2. ANALYSIS OF TRADITIONAL BRANCH-LINE DIFFERENTIAL BANDPASS FILTER

Figure 1(a) depicts the transmission-line schematic of an N-order differential bandpass filter based on a modified branch-line structure. All the transmission lines given in Figure 1(a) are about one quarter-wavelength long with respect to the center frequency (f_0), and the characteristic impedances are Z_T and Z_S, respectively. Under differential- or common-mode operation, the filter in Figure 1(a) can be decomposed into two bisections with respect to a perfect electric or magnetic wall at the symmetrical line AA', which are illustrated in Figures 1(b) and (c).

For the differential-mode bisection, it consists of shunt-connected, short-circuited stubs, each with a length of $\lambda_g/4$ and characteristic impedance of Z_S, coupled via connecting lines of equal $\lambda_g/4$ length and characteristic impedance of Z_T. Here, λ_g denotes the guided wavelength within the propagation medium at the center frequency f_0. According to [21], the differential-mode bisection exhibits bandpass responses at $(2n-1)f_0$ $(n = 1, 2, 3, \ldots)$. For the common-mode bisection, it is constructed by shunt-connected, open-circuited stubs, each with a length of $\lambda_g/4$ and characteristic impedance of Z_S, coupled via connecting lines of equal $\lambda_g/4$ length and characteristic impedance of Z_T. According to [21], the common-mode bisection demonstrates bandstop responses at $(2n-1)f_0$ $(n = 1, 2, 3, \ldots)$.

Ideal transmission coefficients of the structures with different filter orders N shown in Figures 1(b) and (c) are given in Figure 2. As depicted in Figure 2, the differential-mode bisection displays three distinct passbands centered at f_0, $3f_0$, and $5f_0$. These passbands correspond to the first three resonant frequencies of the $\lambda_g/4$ uniform impedance resonators employed in the filter design. In addition, the filter naturally produces four transmission zeros respectively situated at DC, $2f_0$, $4f_0$,

and $6f_0$. These transmission zeros are instrumental in improving the filter's performance, as they create steep transitions between passbands and stopbands. Thus, differential-mode bisection shows outstanding performance in terms of band-to-band isolation and selectivity.

For the common-mode bisection, it presents bandstop response at f_0, $3f_0$, and $5f_0$, which is consistent with the analysis given above. Besides, as shown in Figure 2, the 1 dB bandwidth of each differential-mode passband remains roughly the same under different circuit orders. Furthermore, with the increase of circuit order, the selectivity of the differential-mode passband increases. In addition, the suppression bandwidth of common-mode gradually increases as the circuit order increases. Therefore, taking all the above into account, to simplify the design, a second-order circuit ($N = 2$) was chosen for the subsequent filter design.

In order to explore the impact of Z_T and Z_s on the differential bandpass filter, control variable method was adopted for an in-depth investigation of these two parameters. When Z_S is maintained at a constant value, the differential-mode and common-mode transmission coefficients demonstrate stability, showing no significant variation regardless of change of Z_T, which is plotted in Figure 3. Additionally, when Z_T is held constant, the operating bandwidths of the differential-mode bisection broaden gradually with increasing Z_S, while the bandwidth of common-mode suppression narrows progressively as Z_S increases, which is presented in Figure 4. As a result, the influence of Z_T on the differential-mode and common-mode responses of the filter is relatively minor, whereas Z_s has a much greater impact.

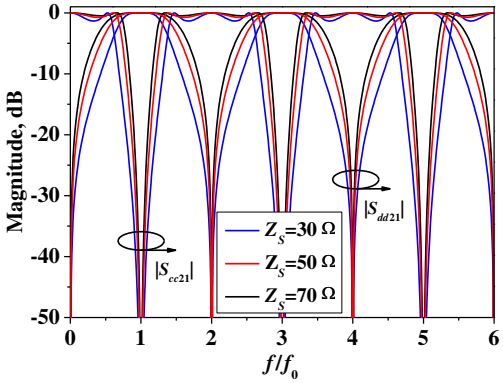

FIGURE 4. Transmission coefficients of bisections shown in Figure 1(b) and (c) with different values of Z_S ($Z_T = 50\,\Omega$).

Consequently, traditional branch-line differential bandpass filter demonstrates superior performance in terms of band-to-band isolation and selectivity for the differential-mode operation and acceptable common-mode rejection. Specifically, the presence of multiple transmission zeros ensures that the filter can effectively attenuate signals outside the desired passbands, thereby enhancing the selectivity and symmetry of the differential-mode passbands.

It is crucial to highlight that, unlike traditional edge-coupled bandpass filters [7–9], which chiefly adjust bandwidth by altering coupling-gap widths, the developed bandpass filter in this design operates differently. It modulates bandwidth by changing the resonator's impedance characteristics, thus avoiding spurious losses from radiation in the coupling gap of conventional designs. To back this claim, Figure 5 presents electric-field distributions in cross-sections of a 50-ohm microstrip transmission line and a pair of 50-ohm coupled transmission lines under comparable operating conditions using a full-wave simulator Ansys HFSS. When being scaled identically, these coupled transmission lines show more energy radiation into the surrounding air. This increased radiation tendency is linked to greater energy dissipation, causing higher insertion loss for the entire device. This observation underscores the significance of the branch-line differential bandpass filter structure. By avoiding reliance on coupling-gap adjustments, it reduces spurious radiation losses, leading to more efficient signal transmission and lower overall insertion loss.

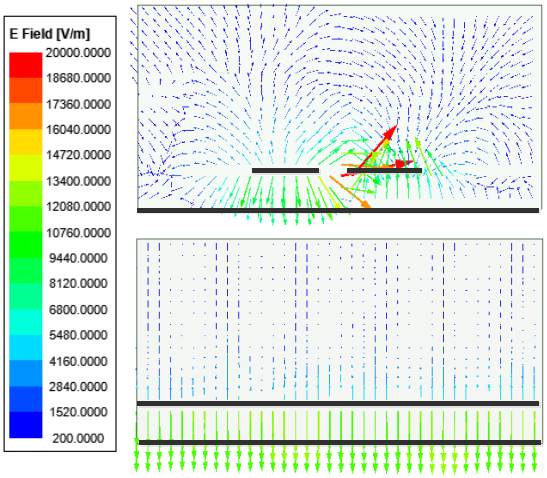

FIGURE 5. Electric field distribution on the cross-section of 50-Ohm microstrip transmission lines and edge-coupled microstrip lines at 1 GHz.

3. DESIGN OF THE TRI-BAND DIFFERENTIAL BANDPASS FILTER

3.1. Analysis of the $\lambda_g/2$ Tri-Section Stepped Impedance Resonators (TSSIRs)

The employed $\lambda_g/2$ TSSIR illustrated in Figure 6 is designed with three distinct characteristic impedances Z_1, Z_2, and Z_3, which is symmetric about line AA'. By applying the symmetrical line as the perfect electric conductor, odd-mode equivalent circuit of the employed $\lambda_g/2$ TSSIR is given in Figure 7. In practical scenarios, it is beneficial to consider that each section possesses an equivalent electrical length. With this premise, the input impedances for the odd-mode equivalent circuit of the employed TSSIR depicted in Figure 7 can be accurately calculated via a sequence of mathematical derivations.

$$Z_{ino1} = jZ_1 \tan\theta \tag{1}$$

$$Z_{ino2} = jZ_2 \frac{Z_2 \tan\theta + Z_1 \tan\theta}{Z_2 - Z_1 \tan^2\theta} \tag{2}$$

$$Z_{ino} = jZ_3 \frac{(Z_1Z_2 + Z_2^2 + Z_1Z_3)\tan\theta - Z_3 \tan^3\theta}{Z_2Z_3 - (Z_1Z_2 + Z_2^2 + Z_1Z_3)\tan^2\theta} \tag{3}$$

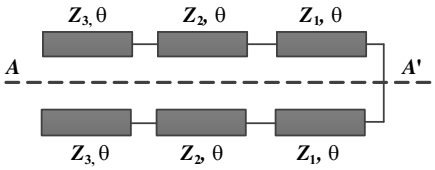

FIGURE 6. Structure of $\lambda_g/2$ TSSIR.

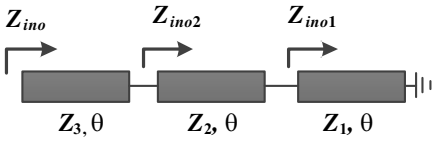

FIGURE 7. Odd-mode equivalent circuit of the employed $\lambda_g/2$ TSSIR.

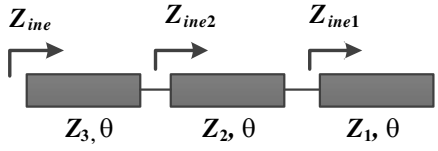

FIGURE 8. Even-mode structure of $\lambda_g/2$ TSSIR.

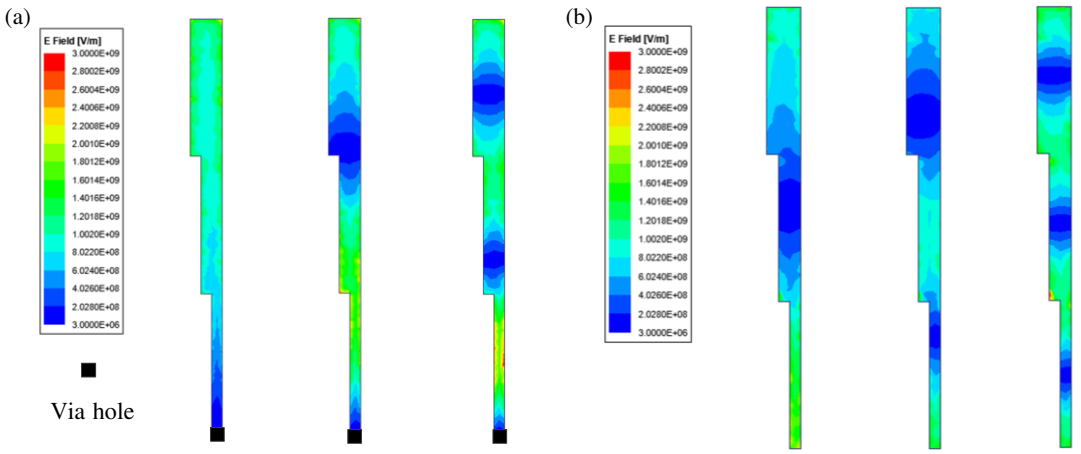

FIGURE 9. Electric field distribution diagrams corresponding to the first three resonant frequencies of the equivalent circuits for the odd and even modes of the TSSIR, (a) odd mode, (b) even mode.

As a result, the condition for the first three resonances of the odd-mode equivalent circuit of this TSSIR can be determined as follows:

$$\theta_{o1} = \theta_o = \tan^{-1}\sqrt{\frac{K_1K_2}{1+K_1+K_2}} \tag{4}$$

$$\theta_{o2} = \frac{\pi}{2} \tag{5}$$

$$\theta_{o3} = \pi - \theta \tag{6}$$

where $K_1 = Z_3/Z_2$, $K_2 = Z_2/Z_1$. When the discontinuity and dispersion effects of the TSSIR have been ignored, the fundamental property of the odd-mode equivalent circuit of the employed TSSIR can be obtained as $f_{o1} : f_{o2} : f_{o3} = \theta_{o1} : \theta_{o2} : \theta_{o3}$. Therefore, once center frequencies f_{o1}, f_{o2}, f_{o3} have been assigned, the required impedance ratios for the TSSIR can be determined using the same method as presented in [22].

In the same manner, when the lengths of the three microstrip lines are identical, the input impedances for the even-mode equivalent circuit of the utilized TSSIR depicted in Figure 8 can be accurately ascertained by employing a systematic sequence of mathematical calculations.

$$Z_{ine1} = -jZ_1\cot\theta \tag{7}$$

$$Z_{ine2} = jZ_2\frac{Z_2\tan^2\theta - Z_1}{(Z_1+Z_2)\tan\theta} \tag{8}$$

$$Z_{ine} = jZ_3\frac{Z_1Z_2 - (Z_2Z_3+Z_2^2+Z_1Z_3)\tan^2\theta}{(Z_1Z_2+Z_2^2+Z_1Z_3)\tan\theta - Z_1Z_2\tan^3\theta} \tag{9}$$

Accordingly, the condition for the first three resonances of the even-mode equivalent circuit of this TSSIR can be determined as follows:

$$\theta_{e1} = \theta_e = \tan^{-1}\sqrt{\frac{1}{K_1K_2+K_1+K_2}} \tag{10}$$

$$\theta_{e2} = \frac{\pi}{2} \tag{11}$$

$$\theta_{e3} = \pi - \theta_e \tag{12}$$

Similarly, when the discontinuity and dispersion effects of the TSSIR have been ignored, the fundamental property of the even-mode equivalent circuit of the utilized TSSIR can be obtained as $f_{e1} : f_{e2} : f_{e3} = \theta_{e1} : \theta_{e2} : \theta_{e3}$.

Electric field distribution diagrams corresponding to the first three resonant frequencies of the equivalent circuits for the odd and even modes of the TSSIR are given in Figure 9. As seen from Figure 9(a), for the fundamental mode of the odd-mode equivalent circuit, it acts as a quarter-wavelength resonator, while the electric fields of its second and third harmonics have one and two zero points, respectively. For the fundamental mode of the even-mode equivalent circuit shown in Figure 9(b), it functions as a half-wavelength resonator, while the electric fields of its second and third harmonics have two and three zero points, respectively.

3.2. Tri-Band Differential Bandpass Filter Design

In order to ensure minimal impedance mismatch between the intermediate transmission line and 50-ohm input/output ports,

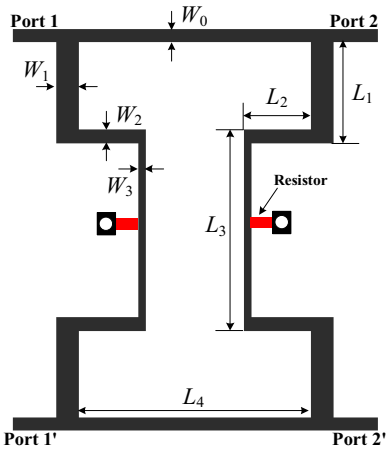

FIGURE 10. Layout of the tri-band differential bandpass filter. (Dimensions: $W_0 = 1.9\,\text{mm}$, $W_1 = 3.3\,\text{mm}$, $W_2 = 2\,\text{mm}$, $W_3 = 1\,\text{mm}$, $L_1 = 10.5\,\text{mm}$, $L_2 = 10.2\,\text{mm}$, $L_3 = 21\,\text{mm}$, $L_4 = 35.4\,\text{mm}$).

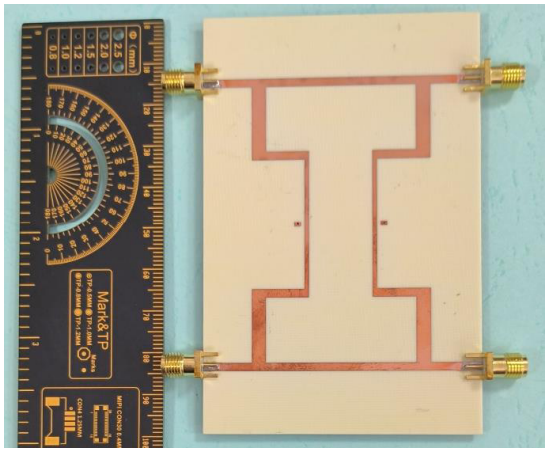

FIGURE 11. Photograph of the tri-band differential bandpass filter.

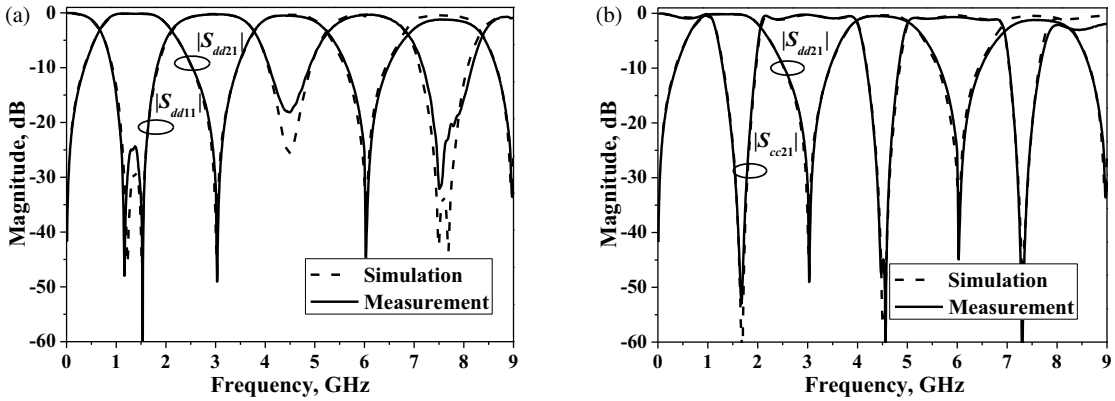

FIGURE 12. Simulated and measured results, (a) differential-mode results, (b) common-mode results.

the characteristic impedance (Z_T) of the transmission line connecting these two TSSIRs is also set to 50 ohms. Expanding on the prior investigation of traditional branch line differentials and TSSIRs and by analogy with the design approaches of standard edge-coupled bandpass filters, the tri-band differential bandpass filter presented in this work, depicted in Figure 10, has been developed. This tri-band differential bandpass filter prototype is constructed on a Rogers 4003C substrate, which has a dielectric constant (ε_r) of 3.55 and a loss tangent ($\tan\delta$) of 0.0027, and the substrate thickness is 32 mil. In accordance with the theoretical analysis detailed in Subsection 3.1, the center frequencies of the three passbands are established at 1.35 GHz, 4.5 GHz, and 7.6 GHz. Consequently, the impedance ratios are determined to be $K_1 = 0.73$ and $K_2 = 0.81$.

The width of the middle section of the proposed $\lambda_g/4$ TSSIR is selected as 1.5 mm, which corresponds to a characteristic impedance of 56 Ω. The characteristic impedances of the other two sections are calculated to be $Z_1 = 69\,\Omega$ and $Z_3 = 41\,\Omega$. Meanwhile, the odd-mode electric length of each section at 1.35 GHz can be calculated as $\theta_o = \theta_{o1} = \theta_{o2} = \theta_{o3} = 25.8°$ while the even-mode electric length of each section at 1.35 GHz can be calculated as $\theta_e = \theta_{e1} = \theta_{e2} = \theta_{e3} = 30.4°$.

3.3. Results

The fabricated tri-band bandpass filter is shown in Figure 11, with its key parameters listed alongside. A detailed comparison between the simulated and measured performances of the proposed tri-band filter is presented in Figure 12. The filter features three distinct passbands centered at 1.35 GHz, 4.5 GHz, and 7.6 GHz. By capitalizing on the advantageous attributes of the conventional filter structure, the measured minimum insertion losses for these passbands are 0.15 dB, 0.5 dB, and 1.2 dB, respectively, including losses from the SMA connectors. Notably, the significant insertion loss in the third passband is primarily attributed to the excessive insertion loss of the SMA connectors at frequencies above 6 GHz, which can be readily observed from Figure 11. Additionally, the presence of transmission zeros at 0 GHz, 3.02 GHz, 6.03 GHz, and 9 GHz significantly improves the selectivity, passband symmetry, and band-to-band isolation of the tri-band filter. Three differential-mode passbands exhibit relative 3-dB bandwidths of 104%, 31%, and 17%, respectively. The isolation between the first and second passbands is 48 dB, while the isolation between the second and third passbands is 45 dB. Specifically, referring to the calculation methods of selectivity (roll-off rate) of filters in [23], the

roll-off rates for the three passbands are as follows: for the first passband, 30 dB/GHz at the lower edge and 23 dB/GHz at the upper edge; for the second passband, 27 dB/GHz at the lower edge and 25 dB/GHz at the upper edge; and for the third passband, 24 dB/GHz at the lower edge and 29 dB/GHz at the upper edge.

Due to the inconsistency of the resonant frequencies of the odd and even modes, the common-mode rejection level is relatively poor and fails to cover the entire 3 dB operating bandwidth. To address this issue, the method of loaded resistors is initially employed to absorb the common mode. Specifically, a resistor was added between the two resonators, and a parametric sweep of the resistor values was conducted, as illustrated in Figure 13. It can be observed from Figure 13 that loading resistors of different values has no impact on the differential-mode response but only adjusts the common-mode rejection. By comparing the common-mode rejection under different resistor values as shown in Figure 13, a resistance value of 40 Ω is ultimately selected.

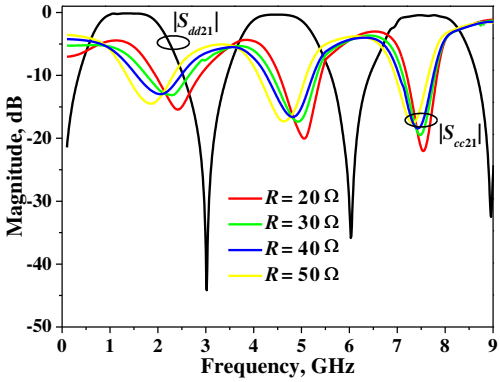

FIGURE 13. Simulated results of transmission coefficients of differential- and common-mode bisection with different values of R.

Photograph, simulated and measured results of transmission coefficients of the developed tri-band differential bandpass filter with loaded resistors are given in Figures 14 and 15, respectively. As depicted in Figure 15, the introduction of loaded resistors results in an increase in the common-mode rejection bandwidth within these three passbands of the differential filter. However, this modification also leads to a significant reduction in the maximum level of common-mode rejection.

As a result, the method of loaded open-circuit stub is employed to adjust the common-mode resonant frequencies. This approach holds the advantage of not significantly affecting the maximum value of common-mode rejection. Specifically, an open-circuit stub added to the center of one of utilized TISIRs, and a parametric sweep of the length and width of the loaded stub is carried out, as illustrated in Figure 16. According to Figure 16(a), it can be observed that once the width of the open-circuit stub is determined, altering its length has essentially no impact on the common-mode suppression of the first two passbands; however, it does adjust the level of common-mode suppression for the third passband. As depicted in Figure 16(b), once the length of the open-circuit stub is set, varying its width only affects the common-mode suppression level of the first passband, with minimal effect on the common-mode suppression of the other two passbands. Similarly, the loading of the open-circuit branch does not influence the differential mode correspondence. Consequently, taking into account the aforementioned outcomes, the length and width of the open-circuit stub are selected to be $L = 10$ mm and $W = 1.5$ mm.

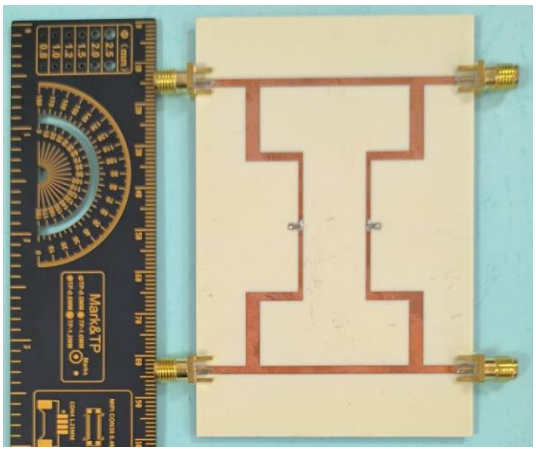

FIGURE 14. Photograph of the developed tri-band differential bandpass filter with loaded resistors.

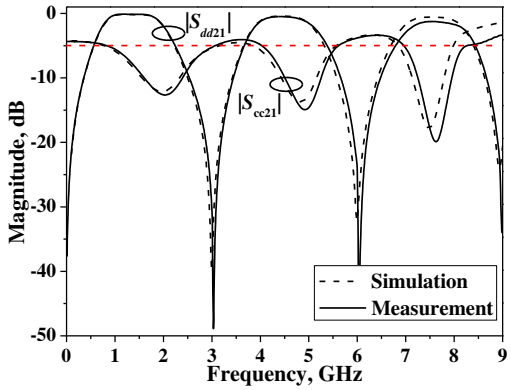

FIGURE 15. Simulated and measured results of transmission coefficients of differential- and common-mode bisection with loaded resistors.

Photograph, simulated and measured results of transmission coefficients of the proposed tri-band differential bandpass filter with a loaded open-circuit stub are given in Figures 17 and 18, respectively. As can be seen in Figure 18, the incorporation of the loaded open-circuit stub leads to an expansion of the common-mode rejection bandwidth within the three passbands of the differential filter. In comparison with Figure 12, the introduction of open-circuit stubs essentially has no effect on the maximum common-mode rejection performance within the passbands. Compared to the method of loading resistors, this approach not only broadens the common-mode rejection bandwidth but also does not affect the maximum common-mode rejection performance.

Performance summary of the proposed tri-band differential bandpass filter and state-of-the-art designs are tabulated in Table 1. As can be seen from Table 1, the insertion loss of the present design is significantly lower than that of the designs based on the PCB process reported in [7–12]. Com-

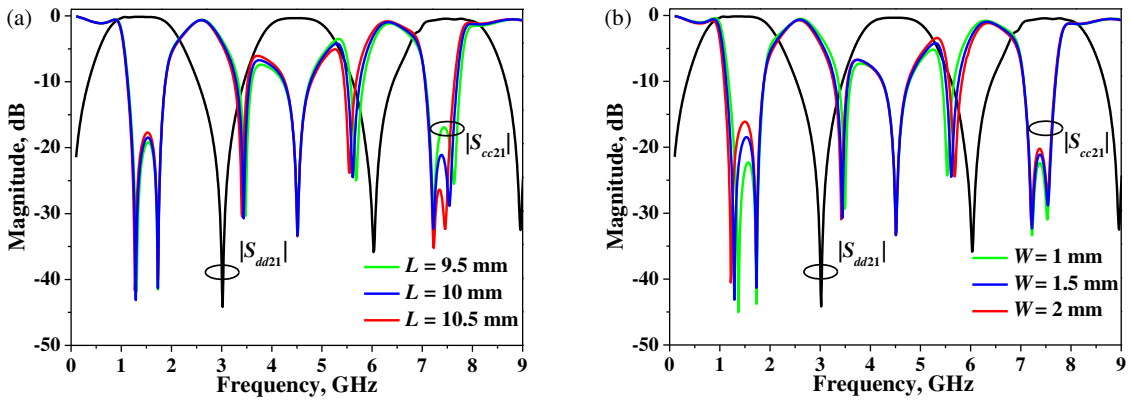

FIGURE 16. Simulated results of transmission coefficients of differential- and common-mode bisection with loaded open-circuit stub, (a) Different length L ($W = 1.5$ mm), (b) Different width W ($L = 10$ mm).

TABLE 1. Performance summary of the proposed tri-band differential bandpass filter and state-of-theart designs.

REF.	f_{01}, f_{02}, f_{03} (GHz)	IL (dB)	CM suppression	Multi order	Layer/ Process	Passband Symmetry Rate	Size ($\lambda_g \times \lambda_g$)
[7]	2.45, 3.50, 5.25	0.71, 0.92, 0.67	$>$ 20 dB	Yes	Single PCB	1.21/1.17/1.35	0.56×0.43
[8]	1.23, 2.39, 3.5	1.09, 2.15, 1.33	$>$ 15 dB	No	Single PCB	1.18/1.41/1.23	0.58×0.19
[9]	2.5, 3.5, 5.8	0.8, 2.3, 2.4	$>$ 31 dB	No	Dual PCB	1.23/1.36/1.31	0.38×0.18
[10]	2.4, 3.5, 5.2	2.43, 3.5, 3.6	$>$ 32 dB	No	Dual PCB	1.32/1.38/1.26	NA
[11]	2.45, 3.5, 4.45	1.44, 1.68, 2.16	$>$ 40 dB	No	Dual PCB	1.41/1.22/1.33	0.68×0.29
[12]	1.57, 2.45, 3.5	1.86, 0.98, 1.49	$>$ 42 dB	No	Dual PCB	1.22/1.33/1.31	0.42×0.2
[19]	1.65, 2.45, 3.50	0.082, 0.11, 0.12	$>$ 36 dB	Yes	Single HTS	1.13/1.25/1.22	0.34×0.26
[20]	1.56, 4.21, 5.79	0.18, 0.19, 0.18	$>$ 32 dB	Yes	Single HTS	1.16/1.21/1.23	0.26×0.15
Work I	1.35, 4.5, 7.6	0.15, 0.5, 1.2	$>$ 5 dB	Yes	Single PCB	1.09/1.12/1.17	0.42×0.32
Work II			$>$ 10 dB				
Work III			$>$ 33 dB				

λ_g: The guide wavelength at the center frequency of the first passband.

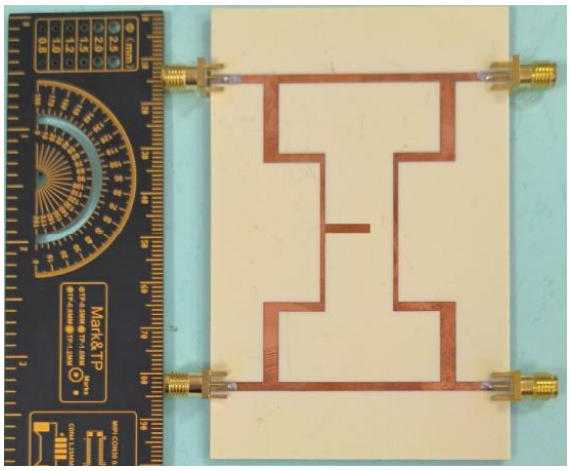

FIGURE 17. Photograph of the developed tri-band differential bandpass filter with a loaded open-circuit stub.

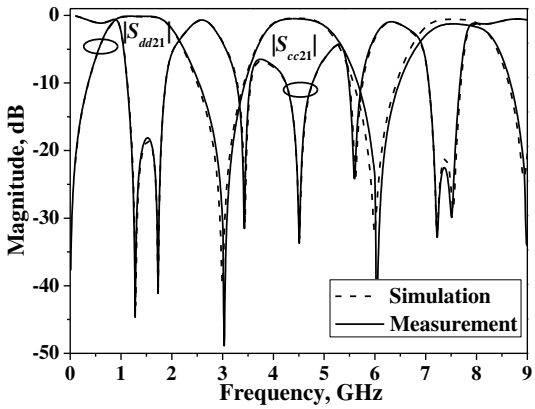

FIGURE 18. Simulated and measured results of the developed tri-band differential bandpass filter with a loaded open-circuit stub.

pared with the tri-band differential filters based on HTS materials [19, 20], the insertion loss of the present design remains comparable. This is because the low insertion loss in HTS filters mainly stems from their significantly lower surface resistance at microwave frequencies and low-temperature operation, which minimizes conductor and material losses.

For a bandpass filter, the passband symmetry can be quantified as follows: As shown in Figure 19, the center frequency of the filter is f; the lower passband edge corresponding to the -10 dB level is f_L; and the upper passband edge corresponding to the -10 dB level is f_H. For an ideal bandpass filter, the symmetry condition can be expressed as $f_H - f = f - f_L$, and passband symmetry ratio (r) can be expressed as $r = (f_H - f)/(f - f_L) = 1$. This metric provides a clear and quantitative measure of the passband symmetry.

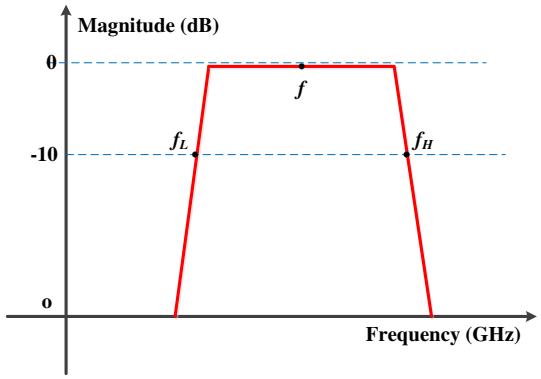

FIGURE 19. Transmission coefficient of a bandpass filter.

However, for commonly used bandpass filters, it is challenging to achieve $r = 1$. But the closer the value of r is to 1, the better the passband symmetry of the filter is. Therefore, we define the passband symmetry ratio r as:

$$r = \frac{\max[(f_H - f), (f - f_L)]}{\min[(f_H - f), (f - f_L)]} \tag{13}$$

Under this definition, the value of r is always greater than 1, which facilitates comparison. As indicated in Table 1, the passband symmetry ratio for each passband of the three bandpass filters presented in this paper is below 1.2, which demonstrates that the design achieves excellent passband symmetry.

For common-mode suppression, the maximum common-mode rejection level within the passbands of differential filters based on single-layer circuit structures generally reaches around 30 dB. In contrast, for designs integrating microstrip lines with slot lines in [9–12], the common-mode suppression level can exceed 40 dB. Moreover, the proposed design is amenable to cascading to achieve higher filter orders, thereby enabling a broader bandwidth and enhanced passband selectivity. This capability is particularly advantageous, as it is challenging to realize multi-order designs in some other approaches [10–12]. Of greater significance is the fact that the symmetry of the three passbands in the present design is notably enhanced, attributable to the presence of transmission zeros between passbands and the inherent structural characteristics. It is worth noting that all the filters designed in this paper are based on single-layer PCB processes. Compared to the filters mentioned above that are based on multilayer PCBs and HTS structures, the filters in this paper demonstrate lower complexity and manufacturing costs. This highlights the practical advantages of our approach in terms of ease of fabrication and cost-effectiveness.

4. CONCLUSION

This paper introduces a differential triple-band bandpass filter designed based on branch-line structures. Four inherently generated transmission zeros within the differential passbands ensure that the isolation between passbands exceeds 45 dB, thereby significantly enhancing the selectivity of the three differential passbands, with roll-off rates at the edges of each passband exceeding 23 dB/GHz. Additionally, the non-edge-coupled configuration employed in the design effectively minimizes additional radiation losses and results in low insertion loss. Specifically, the insertion losses for the three passbands, including the SMA connectors, are 0.15 dB, 0.5 dB, and 1.2 dB, respectively. Furthermore, another advantage brought by the non-edge-coupled structure is that it mitigates the impact of processing tolerances on the actual circuit, resulting in excellent agreement between simulation and measurement outcomes.

ACKNOWLEDGEMENT

This work was supported by the National Natural Science Foundation of China under Grants 62201291, Natural Science Research Project of Jiangsu Higher Education Institutions (Grant 23KJD510002) and Natural Science and Technology Project of Jiangsu College of Engineering and Technology (Grant GYKY/2024/5, Grant JSGYZRJJZD-03).

REFERENCES

[1] Song, Y., H. Liu, L. Feng, C. Guo, S. Zheng, and Z. Ma, "High-order balanced dual-band HTS BPF with flexible frequency ratio and sharp rejection skirts," *IEEE Transactions on Microwave Theory and Techniques*, Vol. 70, No. 4, 2185–2195, 2022.

[2] Song, Y., H. Liu, L. Feng, and H. Xu, "Balanced dual-band HTS BPF with controllable frequency ratio and transmission zeros using mixed cross-coupling," *IEEE Transactions on Circuits and Systems II: Express Briefs*, Vol. 69, No. 11, 4313–4317, 2022.

[3] Chen, J.-X., Y. Xue, X. Shi, Y.-X. Huang, W. Qin, and Y.-J. Yang, "Design of double-ridge waveguide balanced filter and filtering power divider," *IEEE Transactions on Microwave Theory and Techniques*, Vol. 72, No. 10, 5929–5937, 2024.

[4] Zhang, C.-Y., X. Shi, Y.-H. Zhu, Y. Xue, and J.-X. Chen, "A compact interlaced-double-ridge waveguide balanced filter with wideband CM suppression," *IEEE Microwave and Wireless Technology Letters*, Vol. 35, No. 2, 169–172, 2025.

[5] Shi, J. and Q. Xue, "Dual-band and wide-stopband single-band balanced bandpass filters with high selectivity and common-mode suppression," *IEEE Transactions on Microwave Theory and Techniques*, Vol. 58, No. 8, 2204–2212, 2010.

[6] Shi, J. and Q. Xue, "Novel balanced dual-band bandpass filter using coupled stepped-impedance resonators," *IEEE Microwave and Wireless Components Letters*, Vol. 20, No. 1, 19–21, 2010.

[7] Liu, H., Z. Wang, S. Hu, H.-X. Xu, and B. Ren, "Design of tri-band balanced filter with wideband common-mode suppression and upper stopband using square ring loaded resonator," *IEEE Transactions on Circuits and Systems II: Express Briefs*, Vol. 67, No. 10, 1760–1764, 2020.

[8] Zhang, S.-X., Z.-H. Chen, and Q.-X. Chu, "Design of tri-band balanced bandpass filter with controllable frequencies and bandwidths," in *2017 IEEE MTT-S International Microwave Symposium (IMS)*, 1823–1825, Honolulu, HI, USA, 2017.

[9] Wei, F., Y. J. Guo, P.-Y. Qin, and X. W. Shi, "Compact balanced dual-and tri-band bandpass filters based on stub loaded resonators," *IEEE Microwave and Wireless Components Letters*, Vol. 25, No. 2, 76–78, 2015.

[10] Zhang, S.-X., L.-L. Qiu, and Q.-X. Chu, "Multiband balanced filters with controllable bandwidths based on slotline coupling feed," *IEEE Microwave and Wireless Components Letters*, Vol. 27, No. 11, 974–976, 2017.

[11] Yang, Y., Z. Wang, L. Xu, and Y. Liu, "A balanced triband bandpass filter with high selectivity and controllable bandwidths," *International Journal of RF and Microwave Computer-Aided Engineering*, Vol. 29, No. 12, e21976, 2019.

[12] Chen, L., J. Y. Peng, M. Wang, T. T. Zhang, and F. Wei, "Compact balanced tri-band bandpass filter based on stub loaded resonator with high selectivity," *International Journal of RF and Microwave Computer-Aided Engineering*, Vol. 31, No. 12, e22911, 2021.

[13] Lin, S., M. Wang, K. Xu, and L. Zhang, "A low-profile dielectric resonator filter with wide stopband for high integration on PCB," *Micromachines*, Vol. 14, No. 9, 1803, 2023.

[14] Zhou, L.-H., J.-X. Chen, and Q. Xue, "Design of compact coaxial-like bandpass filters using dielectric-loaded strip resonator," *IEEE Transactions on Components, Packaging and Manufacturing Technology*, Vol. 8, No. 3, 456–464, 2018.

[15] Cai, R., C. Shao, and K. Xu, "A low-profile balanced dielectric resonator filtering power divider with isolation," *Micromachines*, Vol. 16, No. 1, 88, 2025.

[16] Chen, J.-X., Y. Zhan, W. Qin, Z.-H. Bao, and Q. Xue, "Analysis and design of balanced dielectric resonator bandpass filters," *IEEE Transactions on Microwave Theory and Techniques*, Vol. 64, No. 5, 1476–1483, 2016.

[17] Roshani, S. and S. Roshani, "A compact coupler design using meandered line compact microstrip resonant cell (MLCMRC) and bended lines," *Wireless Networks*, Vol. 27, No. 1, 677–684, 2021.

[18] Mohamadpour, G., S. Karimi, and S. Roshani, "Design of miniaturized 90-degree hybrid coupler with wide rejection Band using neural network," *Micromachines*, Vol. 15, No. 5, 657, 2024.

[19] Zhang, J., Q. Liu, H. Liu, D. Zhang, and D. Zhou, "Compact balanced tri-band superconducting band-pass filter using double square ring loaded resonators," *International Journal of RF and Microwave Computer-Aided Engineering*, Vol. 31, No. 3, e22530, 2021.

[20] Ren, B., X. Liu, X. Guan, and Z. Ma, "High-selectivity high-temperature superconducting triband balanced bandpass filter using symmetric stub-loaded resonator," *IEEE Transactions on Applied Superconductivity*, Vol. 33, No. 8, 1–5, 2023.

[21] Hong, J.-S. G. and M. J. Lancaster, *Microstrip Filters for RF/Microwave Applications*, John Wiley & Sons, New York, NY, USA, 2004.

[22] Hsu, C., C.-H. Lee, and Y.-H. Hsieh, "Tri-band bandpass filter with sharp passband skirts designed using tri-section SIRs," *IEEE Microwave and Wireless Components Letters*, Vol. 18, No. 1, 19–21, 2008.

[23] Yin, L., Z. Xue, W. Ren, Q. Lv, B. Zhang, and C. Jin, "High-roll-off-rate ultrathin polarization-rotating frequency selective surface," *IEEE Antennas and Wireless Propagation Letters*, Vol. 22, No. 7, 1592–1596, 2023.